https://doi.org/10.5194/egusphere-2025-2857
Preprint. Discussion started: 7 July 2025

A comparison of methods to compute the rate of horizontal geomagnetic field variation

Samuel A. Fielding[1], Philip W. Livermore[3], Ciarán D. Beggan[2], Kathryn A. Whaler[1], and Gemma S. Richardson[2]

[1]School of GeoSciences, University of Edinburgh, Grant Institute, James Hutton Rd, King's Buildings, Edinburgh, United Kingdom EH9 3FE
[2]British Geological Survey, Lyell Centre, Research Avenue South, Edinburgh, United Kingdom EH14 4AP
[3]School of Earth and Environment, University of Leeds, Leeds, United Kingdom LS2 9JT

Correspondence: Samuel A. Fielding (sfieldin@ed.ac.uk)

Abstract. The rate of change of the horizontal external magnetic field is often used as a proxy for space weather activity and in particular for estimating geomagnetically induced currents (GICs) in high voltage power grids. This paper compares two commonly adopted methods for computing this rate of change: (1) the difference between consecutive measurements in the magnitude of the horizontal magnetic field, H', and (2) the combined difference in the magnitude in the northward and eastward directions, usually denoted R. We find that there can be an absolute difference in the calculations between the two methodologies exceeding 100 nT/min during storm times for observatories in the sub-auroral zone, demonstrating that the choice between R and H' can make a significant difference to any GIC estimate. We also note an observable difference between the two methodologies during quiet times when the measurements are made close to the agonic line, though this difference does not have a significant impact on the efficacy of either of the two methodologies for GIC studies. Future studies should consider carefully the choice of geomagnetic indicators for estimation of GICs.

1 Introduction

Research into space weather and the effects from time-varying environmental conditions in the near-Earth environment has grown enormously in the past two decades. As the primary driver, the Sun generates physical phenomena such as, but not limited to, Coronal Mass Ejections which can strongly perturb the Earth's magnetic environment causing effects on modern technology (e.g. Mishra and Teriaca, 2023). Other potentially damaging space weather effects on technology come from solar flares (e.g. Grodji et al., 2022) and solar energetic particles (e.g. Usoskin and Kovaltsov, 2012). At the boundary of the interplanetary magnetic field (IMF) and the geomagnetic field, termed the magnetopause, energy is transferred through to the Earth's magnetosphere, principally through the process of reconnection (Dai et al., 2024; Zhang et al., 2023). The response energizes the radiation belts and enhances ionospheric currents (Case et al., 2021), often causing a visible glow of the upper atmosphere known as the aurora (Gurram et al., 2021). Energy stored and released by the magnetotail produces bursts of geomagnetic activity, called substorms, which drive large rates of change of the external magnetic field which in turn creates measurable variations in magnetic field measurements on the surface (Kanekal and Miyoshi, 2021).

https://doi.org/10.5194/egusphere-2025-2857
Preprint. Discussion started: 7 July 2025

Rapid geomagnetic disturbances induce a subsurface geoelectric field which, if sufficiently intense, can create Geomagnetically Induced Currents (GICs) in low resistance grounded technical infrastructure such as high voltage power grids (Pulkkinen et al., 2005). Geomagnetic disturbances are primarily driven by currents in the magnetosphere and ionosphere especially the auroral electrojet at mid to high latitudes (Pulkkinen et al., 2017), though the equatorial electrojet and the ring current can also contribute to field variations at lower latitudes (de Villiers et al., 2017). It is possible to interpret the magnetic field variation by modeling the electric field producing the magnetic field as two current systems, one externally-driven current system including ionospheric currents, and one internally induced in the shallow subsurface. The externally driven current system dominates in auroral areas, though the internal component can contribute up to 30% of a given perturbation (Juusola et al., 2020). In extreme storms, depending on local geology, geoelectric fields can reach over 10 V/km in regions with high subsurface resistivity (Kelbert and Lucas, 2020).

GICs are effectively quasi-DC in power grids and other critical infrastructure networks which can pose a significant economic hazard as they affect transformer operation, particularly through saturation of the hysteresis loop (Oughton et al., 2018; Rajput et al., 2021; Ramírez-Niño et al., 2016). Half-cycle saturation generates even harmonics, enhanced reactive power consumption and overheating which can cause permanent damage to critical infrastructure (Bolduc, 2002; Boteler, 2019; Abda et al., 2020). Mac Manus et al. (2022) found that between 13% and 35% of transformers in New Zealand were at risk of damage through the impact of GICs. As GIC flow is not routinely monitored in many countries, methods for estimating it via proxy measurements have been developed (Marshall et al., 2011).

The use of the ground-level magnetic field as an indicator of GIC activity relies on the time derivative of the geomagnetic field, and more specifically of the 2D horizontal vector geomagnetic field $\mathbf{B}_H$, the projection of $\mathbf{B}$ in the horizontal plane (Viljanen et al., 2001). As ground-level magnetic field is measured continuously at hundreds of dedicated observatories around the world, it can provide a proxy for regional GIC activity (Smith et al., 2021).

Considering the time derivative of the 2D horizontal vector geomagnetic field rather than the total magnetic field is based on the induction response as used in magnetotelluric sounding. This establishes a frequency-dependent relationship between the magnetic to electric field variations as measured in the North ($\mathbf{B}_N$) and East ($\mathbf{B}_E$) directions (Robertson, 1987). Two standard formulae have been used for computing the horizontal rate of change of the magnetic field from digitised observatory data. In this study, we examine both of these methods for computing the rate of change and the observed differences that arise between them. The next section describes the differences between the two methodologies, followed by sections on the observed and modeled differences between both. We follow this with a discussion related to scenarios where the results from each method can differ by many orders of magnitude.

2 Difference between methods of computing horizontal field change

Representing the horizontal component of the geomagnetic field as a scalar indicator of GIC activity is ambiguous. Consider a digitised time series of orthogonal components of the magnetic field, measured at a permanent magnetic observatory for example. While there is only one correct way to evaluate the first-order time derivative of the magnetic field vector through

https://doi.org/10.5194/egusphere-2025-2857
Preprint. Discussion started: 7 July 2025

subtraction of successive readings, there are there are several methods that can be used to distill the derivative into a scalar value. The scalar magnitude of the horizontal component B_H is defined in terms of the northward and eastward components B_N and B_E:

$$B_H = \sqrt{B_N^2 + B_E^2}. \tag{1}$$

One approach to compute the derivative is take the overall magnitude of the horizontal magnetic field B_H and subtract from it the horizontal magnetic field given by the previous measurement, which written in terms of the northwards and eastwards components B_N and B_E when assuming $\frac{\delta B_H}{\delta t} << B_H$, yields:

$$H' = \frac{\delta B_H}{\delta t} = \frac{1}{B_H} \cdot (B_N \frac{\delta B_N}{\delta t} + B_E \frac{\delta B_E}{\delta t}) = \hat{\mathbf{B}}_H \cdot \frac{\delta \mathbf{B}_H}{\delta t}, \tag{2}$$

where $\hat{\mathbf{B}}$ denotes a unit vector in the direction of the magnetic field and δt is the time difference between successive measurements. Alternatively, one can incorporate the rate of change of the magnetic field in the two perpendicular directions $\mathbf{B}_N$ and $\mathbf{B}_E$ separately using their scalar values B_N and B_E by the quantity R, given by (Smith et al., 2021):

$$R = |\frac{\delta \mathbf{B}_H}{\delta t}| = \sqrt{\left(\frac{\delta B_N}{\delta t}\right)^2 + \left(\frac{\delta B_E}{\delta t}\right)^2}. \tag{3}$$

This means that H' can be written in terms of R:

$$H' = \hat{\mathbf{B}}_H \cdot \frac{\delta \mathbf{B}_H}{\delta t} = |\hat{\mathbf{B}}_H| \cdot |\frac{\delta \mathbf{B}_H}{\delta t}| \cdot \cos\theta = R \cdot \cos\theta \tag{4}$$

where θ is the difference in angle between the perturbation and the original magnetic field magnitude. The two methods, H' and R, give the same value when the perturbation vector $\delta\mathbf{B} = (\delta B_N, \delta B_E)$ is in the same direction as $\mathbf{B}_H$. One difference between the two is that R is always positive whereas H' can take either sign. However, as space weather applications do not necessarily need to take the sign of GICs into account, this is less important in the comparison between the two methodologies, as a decrease in magnetic field strength is just as effective at inducing a geoelectric field as an increase if they have the same absolute value. The two methods can lead to substantially different results when the magnetic field changes rapidly in direction, especially if this directional change is not associated with a change in magnitude. R will always produce an equal or higher value than H', because in equation (4), $\cos\theta \leq 1$. As a result, H' has a lower magnitude than R unless there is no change in the direction of the magnetic field from one measurement to the next, in which case the two methods produce estimates of the same magnitude (though H' may be negative). In the case where $\cos\theta$ is zero (i.e. θ is 90°), equation (4) will give a value of zero for H' but R given by equation (3) will be non-zero.

In equation (2), the components δB_N and δB_E of any perturbation δB_H do not have the same weight, as each is multiplied by the magnitude of the field in that direction. For example, if the field is predominantly in the northward direction (as expected for an axial dipole dominated field), then $B_N >> B_E$ and H' is dominated by the perturbation $\delta B_N/\delta t$. As a contrast, in equation (3), the two components are equally weighted. It is worth noting that geomagnetic field data portals such as INTERMAGNET provide direct access to B_H along with the vertical intensity and declination. With B_H directly available from the portal, the

https://doi.org/10.5194/egusphere-2025-2857
Preprint. Discussion started: 7 July 2025

use of equation (2) to carry out studies into horizontal geomagnetic field perturbation becomes trivial, whereas to calculate R the declination also has to be used to derive the correct magnitude of B_N and B_E.

In addition to considering individual cases when H' and R differ, it is interesting to consider the distribution of H' and R in a large number of trials in each of which the perturbations are randomly drawn. This situation somewhat mimics the geophysical situation where at a given observatory the externally driven field changes may appear quasi-random. In the simplest case, suppose that the perturbations are uniformly distributed in angle and all have the same magnitude. Then H' depends only on the angle between the background field and the perturbation, and because the distribution of the perturbations are rotationally invariant, a histogram of H' will be independent of the direction of the background field, that is, it will look the same at every observatory. Likewise, a histogram of R is independent of background field. Hence, under these assumptions, the distribution of R and H' should be the same everywhere. However, magnetic field perturbations are not uniformly distributed, and there are locations where the background magnetic field is more aligned or less aligned with the externally driven magnetic field perturbations, with this dependence also depending on relative geomagnetic activity (Viljanen et al., 2001). As a result the outputs of the two methods for calculating ground level magnetic field perturbation can in fact be quite different, and will in general depend on location and geomagnetic activity. In the next section, we compute and describe the differences between the two methods using minute-mean data from a set of global observatory measurements. The difference between the methods could have implications for many studies in space weather research (e.g., Thomson et al. (2011); Mac Manus et al. (2017), both using H', and Smith et al. (2021) using R).

Although R and H' are simple measures of horizontal field change, it would be more accurate to model GICs using a convolution integral to incorporate correctly the effect of the finite conductivity of the Earth on GICs, though the conductivity profile is not always available. Viljanen (1998), and Bedrosian (2007), for example, pointed out that the effect of perturbations in the eastwards and northward directions can be treated independently if the geometry of the conductor network (i.e. power grid) impulse response is known. They also noted that the northward magnetic field perturbation dominates GIC activity at stations in Finland for example. The externally driven magnetic field change calculated using the two-dimensional Spherical Elementary Current System (2D SECS) method can also be used as a GIC activity indicator (e.g. Juusola et al., 2023). By including the internal magnetic field component, a dependence on the local conductivity structure of the subsurface would be introduced (Pedersen et al., 2024). This could be a more appropriate indicator of GIC activity than either H' or R if such conductivity data are available.

3 Results

3.1 Observed difference between R and H'

We computed values of both H' and R for 52 geomagnetic observatories from 1998 to 2020 to examine the spatial distribution of differences between these two definitions of horizontal change. The data consist of definitive 1998-2020 INTERMAGNET data (Love and Chulliat, 2013), collected through the VirES server (Smith et al., 2022, 2025). From this dataset, we took the definitive magnetic field components of B_N, B_E and B_H at 1 minute cadence, allowing us to calculate 1 minute resolution

https://doi.org/10.5194/egusphere-2025-2857
Preprint. Discussion started: 7 July 2025

magnetic field derivative estimates. Mean monthly sunspot number was downloaded from SILSO (Clette and Lefèvre, 2015). We also utilize the CHAOS-7 magnetic field model (Finlay et al., 2020) to model the effect of declination and intensity on the difference between the two methodologies.

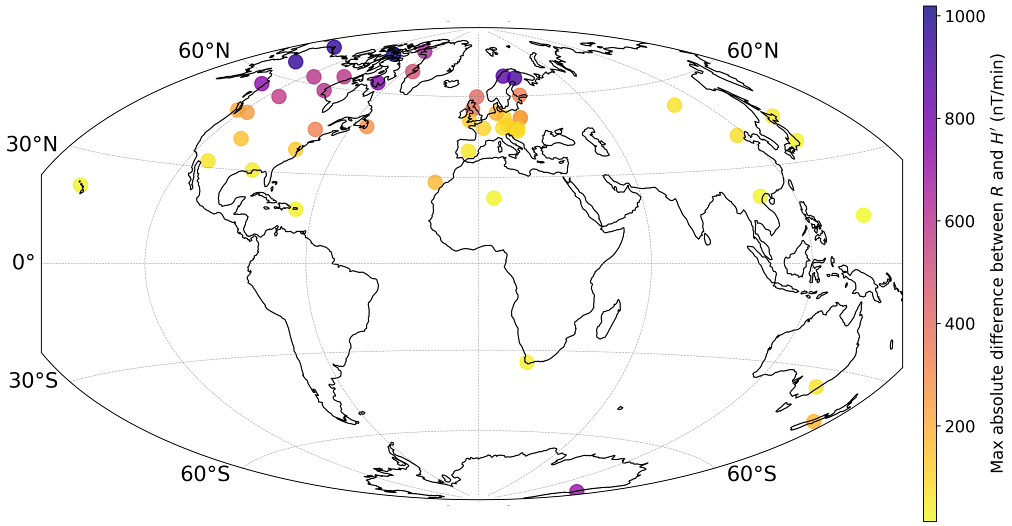

Figure 1. The maximum absolute difference between R and H' at INTERMAGNET observatories from 1998-2020, found by calculating the difference between the two methods at every minute and plotting the greatest absolute difference.

Figure 1 shows the absolute difference between R and H' at 50 observatories, with two observatories omitted due to anomalously high differences (more than 5,000 nT/min, Narsarsuaq (NAQ, 61.17°N, 45.43°W) and Alibag (ABG, 18.64°N, 72.87°E)). We found a clear dependence on latitude for the relationship between R and H'. This is because there is a linear dependence on perturbation size, as from equation (4), $R - H' = R(1 - \cos\theta)$, and average perturbation magnitude increases proportionally to the background horizontal field strength, becoming higher closer to the poles. Three of observatories were chosen for closer investigation as case studies at a variety of latitudes, namely Chambon-la-Forêt, France (CLF, 48.03°N 2.26°E), Tamanrasset, Algeria (TAM, 22.79°N 5.53°E), and Scott Base, Antarctica (SBA, 77.83°S 166.67°E). The statistical properties of H' and R for each of these observatories are displayed in table 1. The largest differences between the methods

https://doi.org/10.5194/egusphere-2025-2857
Preprint. Discussion started: 7 July 2025

Table 1. Statistics of three stations at different latitudes, with data available from 1998-2020. PCC is the Pearson Correlation Coefficient between R and H' over the full period from 1998-2020, and is shown with the mean values of H' and R over the same period.

Observatory	Max difference between R, H'	Date of max difference	PCC	Mean H'	Mean R	Mean $\frac{R}{H'}$
TAM	29 nT/min	5:37 UTC, 31/10/2003	0.93	0.27 nT/min	0.38 nT/min	1.42
CLF	107 nT/min	6:59 UTC 29/10/2003	0.83	0.37 nT/min	0.66 nT/min	1.76
SBA	707 nT/min	6:25 UTC, 29/10/2003	0.79	2.31 nT/min	4.18 nT/min	1.80

occur during storm times, which are more common during solar maxima. This includes a maximum difference of 707 nT/min for SBA on 29 October 2003.

We focus on CLF as a mid-latitude observatory that will have the broadest applicability for the United Kingdom and other countries at subauroral locations. A scatter plot between H' and R at CLF is shown in Figure 2, with a Pearson Correlation Coefficient between the two quantities of 0.83. H' is always less than R, and in particular, large R can occur frequently while H' remains low, which is consistent with equation (4). Figure 3 shows the absolute difference between H' and R at CLF between 1998 and 2020 along with the sunspot number over the same period. Solar maxima correspond to the highest difference between the methodologies, while solar minima (i.e. 2007-2011) consistently are contemporaneous with low values between the methodologies less than 20 nT/min. In the next section, we model the difference between the two quantities R and H' for a given perturbation depending on the declination and inclination of the magnetic field model.

3.2 Modeled difference between between R and H'

To demonstrate the difference between the two methods, we construct a model which estimates both H' and R using a background magnetic field model. At a chosen epoch, we calculate B_N and B_E from the CHAOS-7 magnetic field model (Finlay et al., 2020). We then add a spatially-constant perturbation of the geomagnetic field in the northward and eastward directions $\frac{\delta B_N}{\delta t}$ and $\frac{\delta B_E}{\delta t}$ and use equations (2) and (3) to calculate H' and R on a $1°\times 1°$ resolution grid over all latitudes and longitudes. As R does not depend on B_N and B_E, but only on their time derivatives, R is the same everywhere; however, H' displays significant variability.

Figure 4 shows the result of applying a perturbation of 1 nT/min in an eastward direction on 1 July 2013 at 00:00 UTC, with no perturbation in the northward direction. R is 1 nT/min at every location. In this scenario, as the perturbation is eastwards, a strong northward magnetic field will experience the perturbation as a rotation rather than a change in magnitude, and the eastward contribution to H' will be vanishingly small as in equation (2). As a result, close to the agonic line (where declination is equal to zero, so that the northward magnetic field component dominates), H' is significantly smaller than R (coloured dark blue). Conversely, close to the $\pm$ 90° isogonic lines (where declination is $\pm$ 90°), H' and R become almost equal (coloured

https://doi.org/10.5194/egusphere-2025-2857
Preprint. Discussion started: 7 July 2025

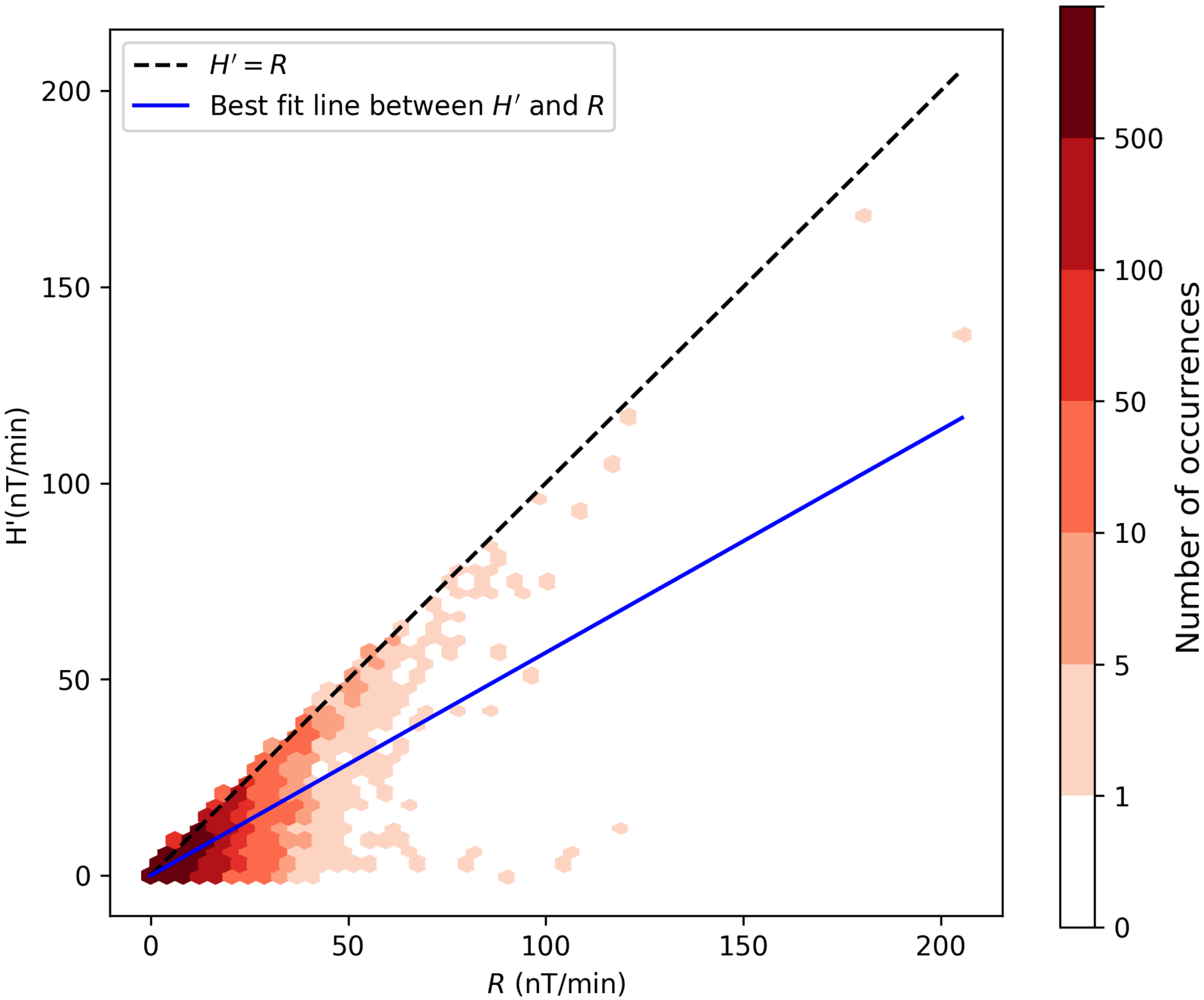

Figure 2. Density plot between H' and R at CLF from 1998 to 2020. The best fit line intercepts the origin, and shows the line where R is 1.76 times larger than H'.

yellow). Figure 4 shows that there can be a significant difference between H' and R, even for the same geomagnetic perturbation, which can result in significant differences between the predicted GIC activity levels, because of the varying angle between $\hat{\mathbf{B}}_H$ and $\frac{\delta \mathbf{B}_H}{\delta t}$.

https://doi.org/10.5194/egusphere-2025-2857
Preprint. Discussion started: 7 July 2025

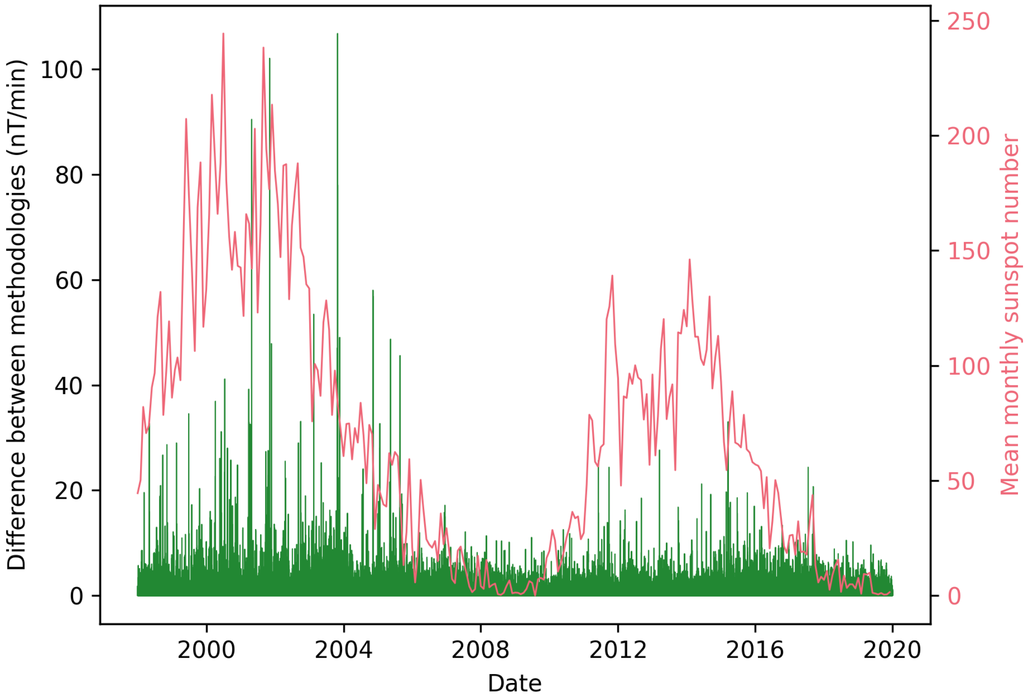

Figure 3. Absolute difference between H' and R for each minute at CLF from 1998-2020 (green) and the mean monthly sunspot number as an indicator of solar activity (pink).

4 Discussion

4.1 Significance of method choice on peak GIC activity

As observed in the previous section, the largest difference between the methodologies at SBA in the time period measured was 707 nT/min, and this difference is typical of high latitude stations. At CLF, the maximum difference was 107nT/min. The effect of such large differences in the rate of change of B_H could be significant for modelling the induced geoelectric current depending on subsurface conductivity. For example, Ingham et al. (2023) inferred an induced geoelectric field in South Island of New Zealand of around 1.5 V/km with a perturbation of 100 nT over an inducing period of 30 seconds. This has the implication that a significantly larger geoelectric field could be predicted when using R compared to H', having direct implications on GIC risk. The greatest difference between H' and R took place during the 2003 Halloween Storm for 17 of the total 52 stations we studied, and 47 of the 52 stations record the greatest difference between the methods when the K_p index (Matzka et al., 2021) is greater than 5. Hence the difference between the methods is largest during storm times, which is when the accuracy of a GIC proxy is the most critical. This would therefore imply that studies into extreme geomagnetic

https://doi.org/10.5194/egusphere-2025-2857
Preprint. Discussion started: 7 July 2025

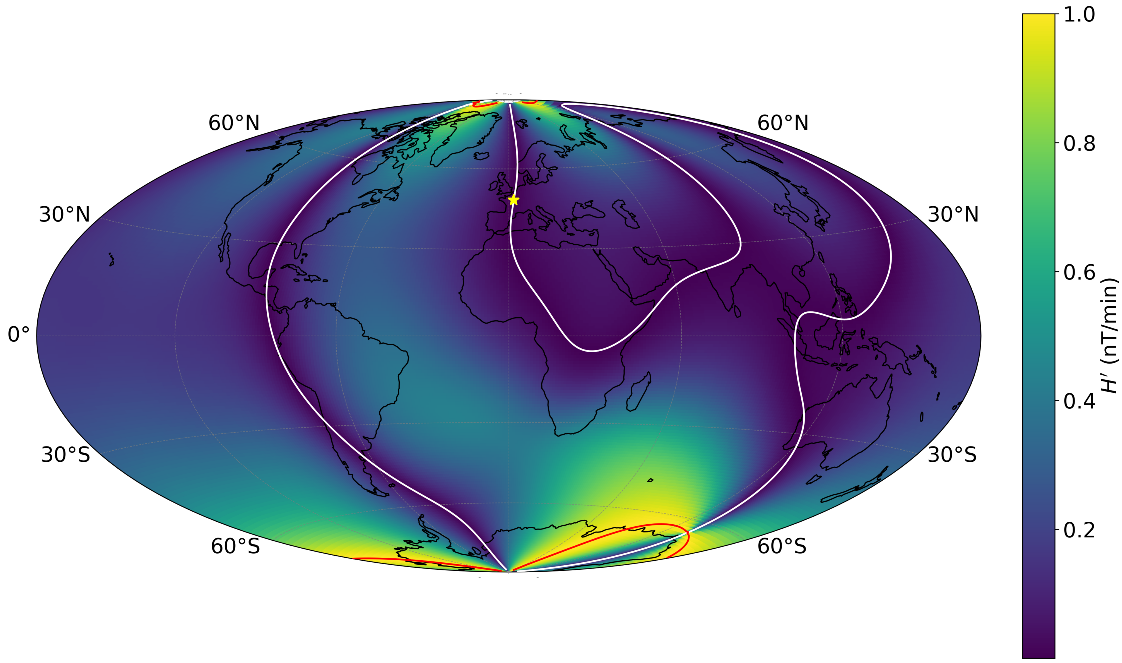

Figure 4. The predicted value of H' for a perturbation of 1 nT/min in an eastward direction using the CHAOS-7 magnetic field model (Finlay et al., 2020) on 1 July 2013 at 00:00 UTC. The white line shows the agonic line and the red lines mark $\pm$ 90° isogonic lines. The yellow star marks the observatory at Chambon-la-Forêt (CLF), France.

activity (e.g. Thomson et al., 2011) may give different results depending on the methodology chosen. Of the five stations that demonstrate the greatest difference when $K_p \leq 5$, four record the greatest difference at midnight UTC possibly due to artifacts in the observatory time series, and the remaining station is Budkov, Czech Republic (BDV, 49.08°N, 14.02°E), recording the highest difference during a disturbance at 12:09 UTC on 1 March 2016. Differences in the two methods are compounded by rapid changes in the declination at storm times (Rastogi, 2005), which contribute to R but not H'.

4.2 Resolution of observatory data and differences between methods close to the agonic line

The resolution of magnetic field data in the northward and eastward directions at any INTERMAGNET observatory is 0.1nT using a vector magnetometer (Bracke, S. (Ed.) and INTERMAGNET Operations Committee and Executive Council, 2025). This is sufficient for measurements of geomagnetic field perturbation during storm times, where the perturbations are orders of magnitude larger than the resolution. This resolution also does not have a significant impact on the efficacy of either H' or

https://doi.org/10.5194/egusphere-2025-2857
Preprint. Discussion started: 7 July 2025

R as indicators of important GICs which would require mitigation or pose a threat to power networks. However, we find that a 0.1nT measurement resolution in combination with the difference between the methods described in the previous section leads to times where R is many orders of magnitude larger than H', in contrast to the typical ratio (1.4–1.8) derived in section 3.1. We therefore comment on this artifact within the data and explain how this discrepancy arises.

During quiet times, measurement resolution is of a similar size to the average geomagnetic field perturbation at 1 minute cadence. Analogue-to-digital conversion causes the data to be quantized in certain values (e.g. Bolic, 2023; Colagrossi et al., 2023). The resolution of magnetic field data has an effect on the directional distribution of the observed geomagnetic field perturbation after analogue to digital conversion, as there are only a finite number of options for a vector measurement on a magnetometer with a certain resolution. This has an effect on the difference between H' and R, as the size of H' is directly affected by the measured magnetic field direction (equation (2)).

We illustrate the effect of the resolution of a geomagnetic observation on the directional distribution of the measured vector magnetic field perturbation. We model the magnetic field as a background field $\mathbf{B_0}$ plus some perturbation vector $\mathbf{P}$. We assume that the background field does not change with time, such that $\mathbf{B_0}$ is arbitrary and has no effect on the perturbation. We then assume that the perturbation has a fixed magnitude and a uniformly-distributed direction. The objective is then to find the measured direction of $\mathbf{P}$ following analogue-digital conversion. We define the perturbation magnitude as P and the resolution as ΔB.

We provide an example, with $P = 2$ and $\Delta B = 1$ in both the north and east directions. In this case, two perturbations at declinations of –10° and 12° from geographic north will produce measured perturbations with northward components of $2\cos(10°)$ and $2\cos(12°)$, with both perturbations producing a measurement of (2,0) in the (north, east) directions after analogue-digital conversion. An angle of 20°, however, will produce a perturbation of $2\cos(20°)$ and $2\sin(20°)$ in the northward and eastward directions, with the digital measurements being rounded to (2,1). This produces a measured perturbation at an angle of 26.6°and a magnitude of $\sqrt{5}$. Perturbation magnitudes can also change significantly during analogue to digital conversion, as illustrated in this example.

In Figure 5, we model perturbations as normally distributed around zero in the northward and eastward directions to produce a illustration of the effect of analogue-digital conversion with as few assumptions as possible. Such a normal distribution is uniform about the mean and has rotational symmetry, which means that there is a uniform directional distribution of perturbation probabilities. This distribution is naïve, as the directional distribution of perturbations are not typically uniform, and the normal distribution will not be representative, especially in active times. However, the distribution allows us to illustrate the effect of digitisation in a controlled fashion.

We take the median perturbation magnitude as 0.45 nT/min, which was the value found for CLF. This was then used to find the corresponding covariance matrix for a bivariate normal distribution with rotational symmetry, which is the identity matrix multiplied by a factor of σ^2. This was found using the Chi-squared distribution with two degrees of freedom (i.e. the Rayleigh distribution), for which the median $m = \sigma\sqrt{2\ln(2)}$, rearranging to give $\sigma^2 = 0.146$ nT/min. We note that San Juan, Puerto Rico (SJG, 18.11°N, 66.15°W) had the lowest median perturbation of any station from 1998-2020 at 0.2 nT/min, producing a potentially even more significant effect in analogue to digital conversion. We then find the measured direction after analogue-

https://doi.org/10.5194/egusphere-2025-2857
Preprint. Discussion started: 7 July 2025

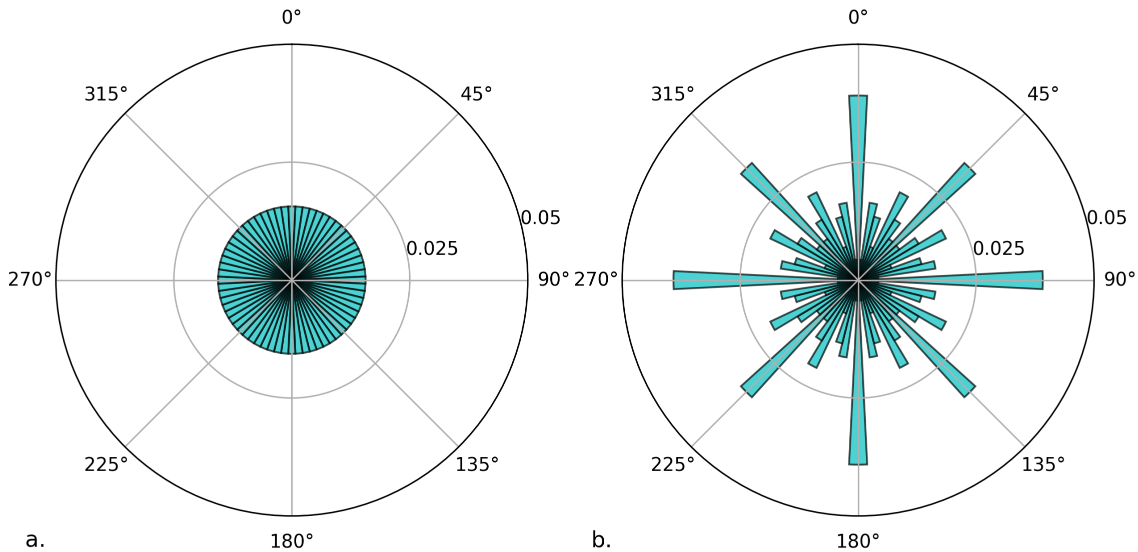

Figure 5. Effect of digitisation. Polar plot of perturbation of the analogue (a.) and digitised (b.) magnetic field when the resolution of the recording equipment is 0.1 nT and the original magnetic field perturbation distribution follows a 2D multivariate (bivariate) normal distribution with the covariance matrix 0.146 I, where I is the identity matrix. This is the covariance matrix for a uniform directional normal distribution with a median of 0.45nT/min (the median magnitude of geomagnetic field perturbation at CLF). The radial axis displays the probability of a certain perturbation being within a given angular bin.

digital conversion. In Figure 5 we plot the probability of a given perturbation falling within each of 64 bins. The plot shows a significant change in the directional distribution favoring directions that are along the axes of measurement (either directly northward or eastward) due to the points (0,1), (0,2) and others. There is also an increase in frequency at 45° due to the point (1,1). The angular width of each bin is 5.625°.

The 0.1 nT resolution of the data changes the directional distribution of digitised magnetic field perturbations compared to those that actually occurred when the resolution is similar to the median magnitude of the geomagnetic perturbation at a given observatory. Perturbations recorded directly in the eastward (for example) directions occur regularly (Figure 5), leading to the recorded magnetic field perturbation in the northward direction during quiet time being measured as 0 nT/min. Close to the agonic line, a perturbation in the eastward direction will have a vanishingly small contribution to H' because the overall magnetic field vector is perpendicular to the magnetic field perturbation (as in equation (2)). This is also true for northward perturbations close to the $\pm$ 90° isogonic lines. An eastwards perturbation close to the agonic line leads to a value of H' which is orders of magnitude smaller than R, demonstrated in Figure 4 with a modeled eastward magnetic field of 1 nT/min. As a result, stations near the agonic line may repeatedly have measurements with $R >> H'$. The agonic line passed through CLF

https://doi.org/10.5194/egusphere-2025-2857
Preprint. Discussion started: 7 July 2025

around mid-2013 giving an opportunity to investigate the effect. The times when the recorded perturbation is directly eastward are highlighted by large values of the ratio Q between R and H'. Q was calculated for each for each measurement (one per

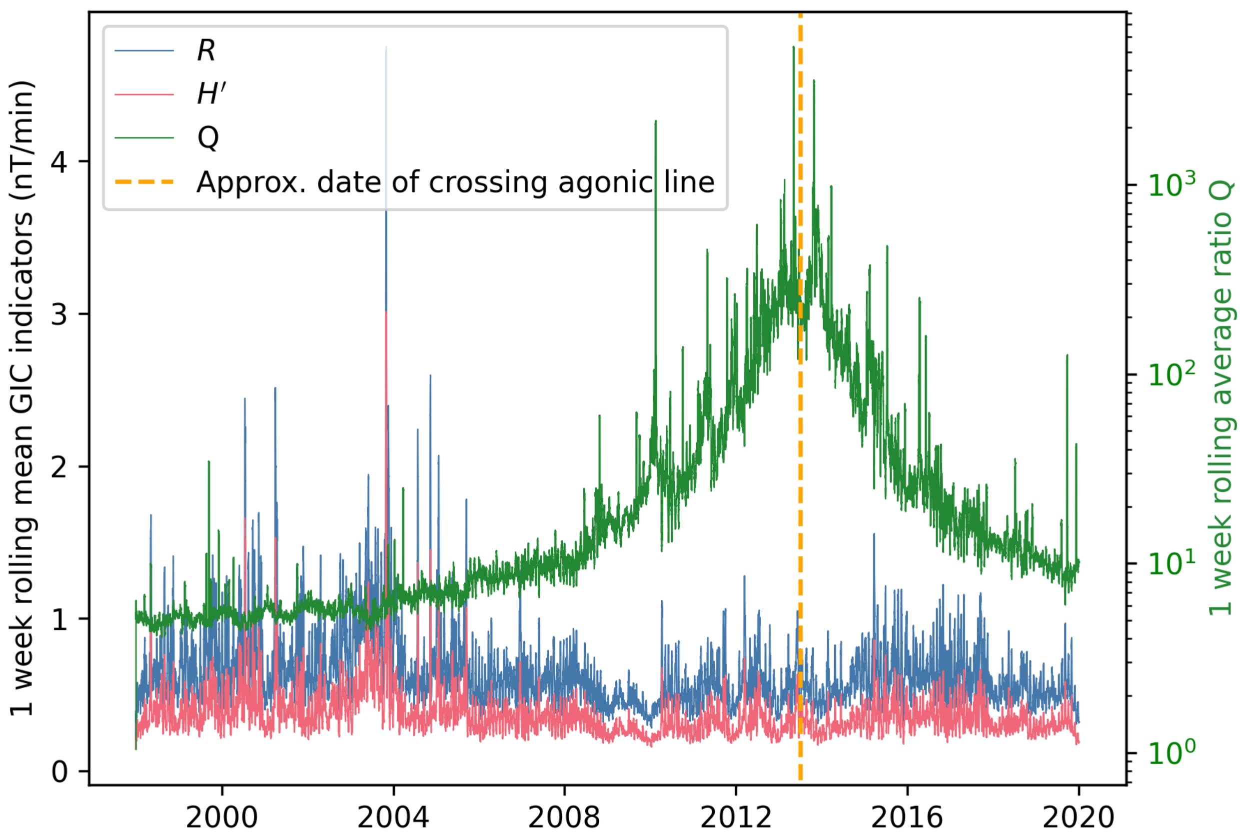

Figure 6. The one-week rolling average (10,080 minutes) of the ratio Q for CLF 1998-2020 (green) alongside the one-week rolling averages of the absolute values of H' (pink) and R (blue). The approximate date the agonic line passed through CLF is in orange (July 2013).

minute), and its rolling average was taken over one week (i.e., 10,080 points at 1 minute cadence) for the full dataset. This allows us to focus on long-term variation. Following from equation (4), $Q = \frac{1}{cos(\theta)}$ for the case where $\frac{\delta B_H}{\delta t} << B_H$, such that the rolling average $Q_{RA}(\tau) = \frac{1}{n}\sum_{t=\tau-n}^{t=\tau}\frac{1}{cos(\theta(t))}$, where n is the number of minutes of data included in the rolling average. The peak in Q shown in Figure 6 corresponds with B_E approaching zero around the period when the agonic line moves westward (Thompson, 1990) through CLF in mid- to late-2013. The value of Q_{RA} greatly exceeds 10 from 2008-2020 and 100

https://doi.org/10.5194/egusphere-2025-2857
Preprint. Discussion started: 7 July 2025

in 2013. Similar results were found at other stations close to the agonic line, including Stennis Space Center, Bay St. Louis, United States (BSL, 30.35°N, 89.64°W) and Fort Churchill, Canada (FCC, 58.76°N, 94.09°W).

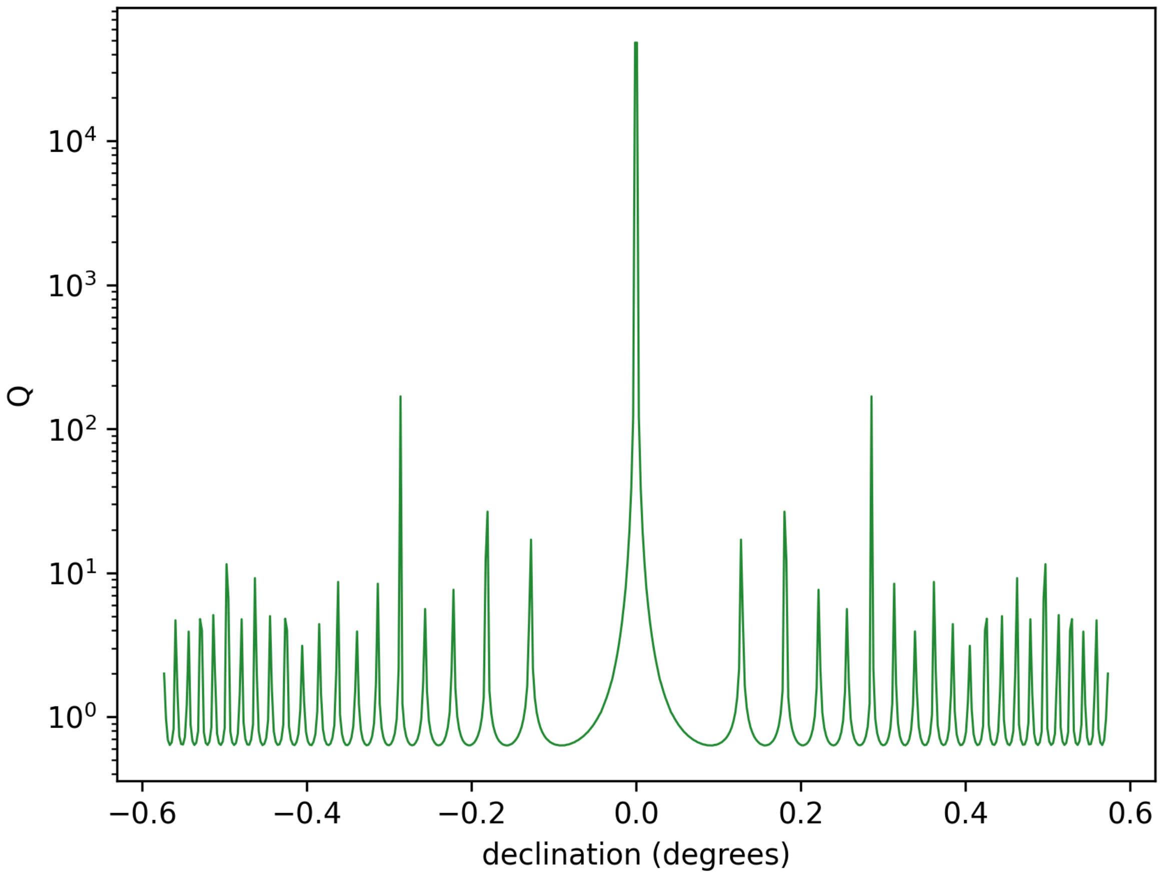

Figure 7. Q for an observatory with a magnetic field intensity of 40,000 nT for a range of declinations around the agonic line assuming the bivariate normal distribution of magnetic field perturbations used to produce Figure 5.

235 Using the directional distribution of magnetic field perturbations described in Figure 5, we can make a prediction of Q as a function of declination for an observatory with a similar total horizontal field intensity as CLF (40,000 nT). We use a bivariate normal distribution to simulate the magnetic field perturbation distribution, with covariate matrix $0.146\mathbf{I}$ as previously noted. Predicted mean Q over the full digitised distribution for a range of declinations is shown in Figure 7, and illustrates that an increase in Q, due to the limited resolution of the file format, is expected around the agonic line, and that other smaller local
240 maxima in Q also exist at other declinations. This corroborates well with Figure 6. The larger range of Q variations in Figure 7

https://doi.org/10.5194/egusphere-2025-2857
Preprint. Discussion started: 7 July 2025

compared with figure 6 is because a bivariate normal distribution is unlikely to be an accurate model of the geomagnetic field perturbation.

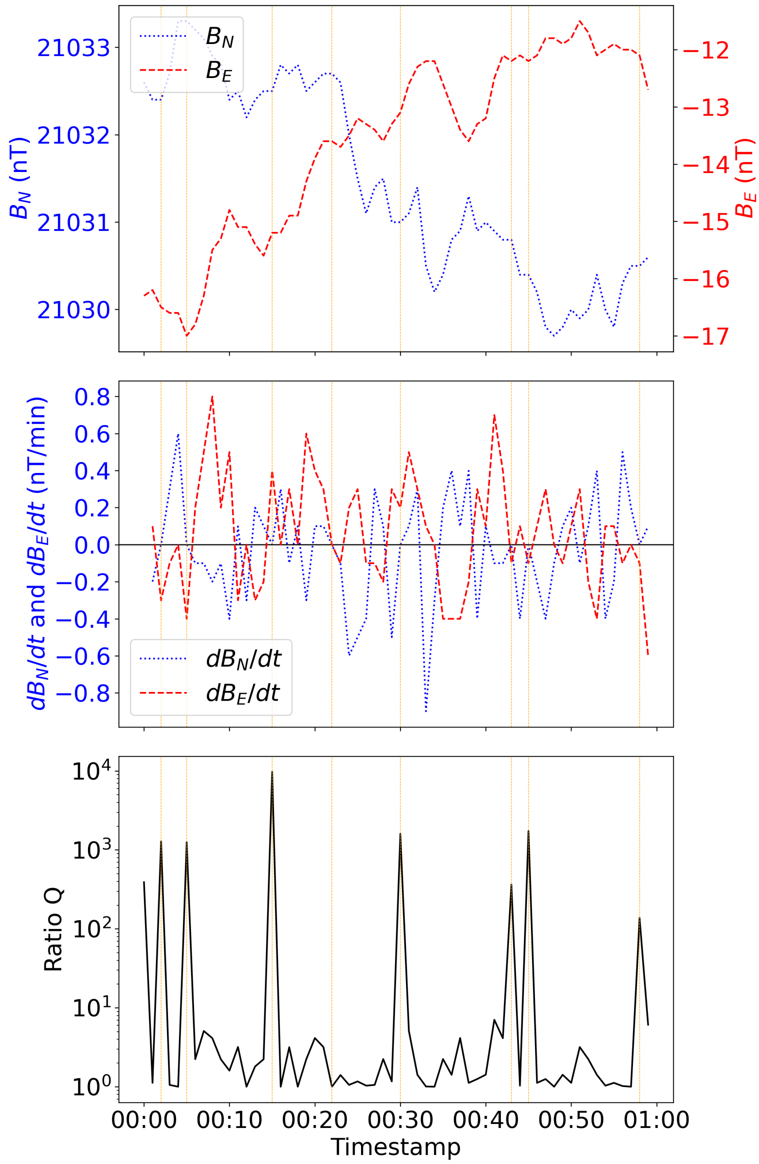

Figure 8. Magnetic field magnitudes B_E and B_N, their derivatives, and the ratio Q between H' and R at CLF for 1 August 2013 between 00:00 UTC and 01:00 UTC. Vertical lines indicate times where $\delta B_N/\delta t$ is equal to zero.

The dominant contributions to large values of Q when the declination is small are measurements where $\frac{\delta B_N}{\delta t}$ vanishes (at the recorded resolution of the observations) and when $\frac{\delta B_E}{\delta t}$ is nonzero. An example of this behaviour is shown in Figure 8,

https://doi.org/10.5194/egusphere-2025-2857
Preprint. Discussion started: 7 July 2025

which is consistent with the hypothesis that high values of Q result from fixed resolution in the file format and proximity to the agonic line. Measurements with the greatest value of Q most commonly coincide with $\frac{\delta B_E}{\delta t}$ also being small (but nonzero), due to smaller perturbations being both more frequent and more influenced by the measurement resolution. Consequently, these intervals do not have a significant contribution to the average absolute difference between H' and R. Again, this is the case for other observatories we investigated close to the agonic line.

To indicate the potential benefits of improving measurement resolution, we calculated the mean deviation between the observed and digitised declination of the magnetic field perturbation as a function of analogue to digital resolution for the bivariate normal distribution with again a covariance matrix of $0.146\mathbf{I}$ as used previously. We found that a resolution of 0.1 nT (shown in Figure 5) leads to a mean deviation in the measurement of declination of 4.12°. These mean deviations would be reduced to 0.45° and 0.01° for resolutions of 0.01 nT and 0.001 nT respectively, both of which would greatly improve the representation of the observed magnetic field data and reduce the difference between H' and R near the agonic line during geomagnetically quiet times.

This investigation implies that the current resolution is having an observable impact on the recorded directional distribution of geomagnetic field perturbations during quiet times, and there are a significant number of instances where no geomagnetic perturbation is recorded in either the northward or eastward directions. We recommend improving the resolution of measurements of the geomagnetic field to 0.01nT to mitigate this artifact. This is feasible with current fluxgate magnetometer systems able to reach a precision of around 10 pT (Bennett et al., 2021).

4.3 Removal of baseline geomagnetic field

The baseline-subtracted horizontal variation field vector $\Delta\mathbf{B}_H$ is a quantity occasionally used to isolate the externally-driven magnetic field and therefore highlight rapid changes, for example in machine learning research (e.g. Madsen et al., 2022). In these studies, the quiet time background magnetic field is removed so that a regression model can predict solely the externally driven part of the measured variation, simplifying the relationship between inputs (i.e. solar wind parameters) and outputs (i.e. rapid variation in ground level magnetic field) to produce a more explainable and more easily trained statistical model. It might be expected that removing the baseline magnetic field before calculating H' has the potential to remove the effect of the relative magnitudes of different magnetic field directions in equation (3). However, we find that subtraction of the baseline geomagnetic field does not qualitatively change the difference between R and H'.

Baseline field subtraction does not change the value of R because it does not depend on the background field. For H' however, the situation is different, and in fact the removal of the baseline can occur either before or after B_H is calculated from B_E and B_N with different effects in each case. Removal of the baseline magnetic field after H' has been calculated introduces an additional term to equation (2) for the rate of change of the magnetic field model. However, this term is vanishingly small compared to the rate of change of the observations, leading to an equation that follows equation (2). This method therefore does not eliminate the difference between H' and R. Alternatively, the baseline magnetic field can be removed before combining B_E and B_N to produce B_H, producing the scalar magnitude of the baseline-subtracted horizontal variation field vector ΔB_H. Following the subtraction of the previous quantity $\Delta B_H(t-\delta t)$ from this quantity to estimate $\frac{\delta(\Delta B_H)}{\delta t}$, the relative contribution

https://doi.org/10.5194/egusphere-2025-2857
Preprint. Discussion started: 7 July 2025

of the horizontal magnetic field perturbation in a given direction is now proportional to the magnitude of the baseline subtracted magnetic field vector $\Delta \mathbf{B}_H$ in that direction since

$$\frac{\delta(\Delta B_H)}{\delta t} = \frac{1}{\Delta B_H} \cdot (\Delta B_N \frac{\delta(\Delta B_N)}{\delta t} + \Delta B_E \frac{\delta(\Delta B_E)}{\delta t}) = \Delta \hat{\mathbf{B}}_H \cdot \frac{\delta}{\delta t}(\Delta \mathbf{B}_H) \tag{5}$$

where ΔB_N and ΔB_E are the northward and eastward components respectively of $\Delta \mathbf{B}_H$. As $\Delta \mathbf{B}_H$ does not have a symmetric directional distribution and has a significantly different distribution to any rapid geomagnetic field perturbation depending on location (Viljanen et al., 2001), removal of the baseline magnetic field does not remove the difference between H' and R. A large geomagnetic perturbation nearly perpendicular to $\Delta \mathbf{B}_H$ will still cause relatively little change in the overall magnitude of $\Delta \mathbf{B}_H$, and will therefore lead to a large discrepancy between H' and R. This means that a machine learning model that uses a baseline subtracted magnetic field variation vector as the target for its training and testing, for example as its GIC indicator, will still give different results depending on which of the two different methods was used to calculate the horizontal magnetic field perturbation.

5 Conclusions

There are two common methods, denoted H' and R, for computing the rate of change of the horizontal magnetic field. H' is calculated by subtracting successive scalar magnitudes of $\mathbf{B}_H$, while R is calculated from the difference between two successive vector measurements of $\mathbf{B}_H$. We show that significant relative and absolute differences can arise between them, particularly during storm times. As a result, calculations of ground level magnetic field perturbations should consider this factor carefully if they are intended as indicators of GIC activity.

We also investigated the relative ratio of H' and R for observatories close to the agonic line. We find that the fixed format of minute mean data to one decimal place can significantly affect the directional distribution of recorded magnetic field perturbations, and has an effect on the computation of H', though this effect is not significant during storm times when GIC activity indicators are the most critical. We recommend improving the resolution of recorded magnetic field data to 0.01nT or better, which will facilitate studies into the directional distribution of magnetic field perturbation.

Data availability. INTERMAGNET data are accessible at https://intermagnet.org/data_download.html, containing all data used for the analyses within this manuscript.

Author contributions. SAF conceptualized the study, made the present analyses and wrote the manuscript with the contribution of the other authors. PL, CB, KW and GR contributed directly to the writing of the manuscript through reviews and edits, were responsible for the structure and style of the manuscript, and assisted with the submission process. PL contributed to the interpretation of the results, contributed

https://doi.org/10.5194/egusphere-2025-2857
Preprint. Discussion started: 7 July 2025

to the structure and message of the paper, and identified the reason for the difference between the two methodologies close to the agonic line. KW supervised the study along with GR, CB and PL.

Competing interests. The authors declare that they have no conflict of interests

Acknowledgements. Funding for this research was provided by NERC through a SENSE CDT studentship (NE/T00939X/1). Additional funding was received from the British Geological Survey (BUFI Number S477) and the United Kingdom Meteorological Office. The results presented in this paper rely on data collected at magnetic observatories. We thank the national institutes that support them and INTERMAGNET for promoting high standards of magnetic observatory practice. (https://www.intermagnet.org/)

https://doi.org/10.5194/egusphere-2025-2857
Preprint. Discussion started: 7 July 2025

References

Abda, Z. M. K., Aziz, N. F. A., Kadir, M. Z. A. A., and Rhazali, Z. A.: A Review of Geomagnetically Induced Current Effects on Electrical Power System: Principles and Theory, IEEE Access, 8, 200 237–200 258, https://doi.org/10.1109/ACCESS.2020.3034347, conference Name: IEEE Access, 2020.

Bedrosian, P. A.: MT+, Integrating Magnetotellurics to Determine Earth Structure, Physical State, and Processes, Surveys in Geophysics, 28, 121–167, https://doi.org/10.1007/s10712-007-9019-6, 2007.

Bennett, J. S., Vyhnalek, B. E., Greenall, H., Bridge, E. M., Gotardo, F., Forstner, S., Harris, G. I., Miranda, F. A., and Bowen, W. P.: Precision Magnetometers for Aerospace Applications: A Review, Sensors, 21, 5568, https://doi.org/10.3390/s21165568, 2021.

Bolduc, L.: GIC observations and studies in the Hydro-Québec power system, Journal of Atmospheric and Solar-Terrestrial Physics, 64, 1793–1802, https://doi.org/10.1016/S1364-6826(02)00128-1, 2002.

Bolic, M.: Chapter 3 - Electronics, in: Pervasive Cardiovascular and Respiratory Monitoring Devices, edited by Bolic, M., pp. 73–123, Academic Press, ISBN 978-0-12-820947-9, https://doi.org/10.1016/B978-0-12-820947-9.00011-8, 2023.

Boteler, D. H.: A 21st Century View of the March 1989 Magnetic Storm, Space Weather, 17, 1427–1441, https://doi.org/10.1029/2019SW002278, 2019.

Bracke, S. (Ed.) and INTERMAGNET Operations Committee and Executive Council: INTERMAGNET Technical Reference Manual, Version a2d1a00, https://tech-man.intermagnet.org/latest/, 2025.

Case, N. A., Hartley, D. P., Grocott, A., Miyoshi, Y., Matsuoka, A., Imajo, S., Kurita, S., Shinohara, I., and Teramoto, M.: Inner Magnetospheric Response to the Interplanetary Magnetic Field B Component: Van Allen Probes and Arase Observations, Journal of Geophysical Research: Space Physics, 126, e2020JA028 765, https://doi.org/10.1029/2020JA028765, 2021.

Clette, F. and Lefèvre, L.: SILSO Sunspot Number V2.0, https://doi.org/10.24414/qnza-ac80, published by WDC SILSO - Royal Observatory of Belgium (ROB), 2015.

Colagrossi, A., Pesce, V., Silvestrini, S., Gonzalez-Arjona, D., Hermosin, P., and Battilana, M.: Chapter Six - Sensors, in: Modern Spacecraft Guidance, Navigation, and Control, edited by Pesce, V., Colagrossi, A., and Silvestrini, S., pp. 253–336, Elsevier, ISBN 978-0-323-90916-7, https://doi.org/10.1016/B978-0-323-90916-7.00006-8, 2023.

Dai, L., Zhu, M., Ren, Y., Gonzalez, W., Wang, C., Sibeck, D., Samsonov, A., Escoubet, P., Tang, B., Zhang, J., and Branduardi-Raymont, G.: Global-scale magnetosphere convection driven by dayside magnetic reconnection, Nature Communications, 15, 639, https://doi.org/10.1038/s41467-024-44992-y, 2024.

de Villiers, J. S., Kosch, M., Yamazaki, Y., and Lotz, S.: Influences of various magnetospheric and ionospheric current systems on geomagnetically induced currents around the world, Space Weather, 15, 403–417, https://doi.org/10.1002/2016SW001566, 2017.

Finlay, C. C., Kloss, C., Olsen, N., Hammer, M. D., Tøffner-Clausen, L., Grayver, A., and Kuvshinov, A.: The CHAOS-7 geomagnetic field model and observed changes in the South Atlantic Anomaly, Earth, Planets and Space, 72, 156, https://doi.org/10.1186/s40623-020-01252-9, 2020.

Grodji, O. D. F., Doumbia, V., Amaechi, P. O., Amory-Mazaudier, C., N'guessan, K., Diaby, K. A. A., Zie, T., and Boka, K.: A Study of Solar Flare Effects on the Geomagnetic Field Components during Solar Cycles 23 and 24, Atmosphere, 13, 69, https://doi.org/10.3390/atmos13010069, 2022.

Gurram, H., Egedal, J., and Daughton, W.: Shear Alfvén Waves Driven by Magnetic Reconnection as an Energy Source for the Aurora Borealis, Geophysical Research Letters, 48, e2021GL094 201, https://doi.org/10.1029/2021GL094201, 2021.

Ingham, M., Pratscher, K., Heise, W., Bertrand, E., Kruglyakov, M., and Rodger, C.: Influence of Tectonic and Geological Structure on GIC in Southern South Island, New Zealand, Space Weather, 21, https://doi.org/10.1029/2023SW003550, 2023.

Juusola, L., Vanhamäki, H., Viljanen, A., and Smirnov, M.: Induced currents due to 3D ground conductivity play a major role in the interpretation of geomagnetic variations, Annales Geophysicae, 38, 983–998, https://doi.org/10.5194/angeo-38-983-2020, 2020.

Juusola, L., Viljanen, A., Dimmock, A. P., Kellinsalmi, M., Schillings, A., and Weygand, J. M.: Drivers of rapid geomagnetic variations at high latitudes, Annales Geophysicae, 41, 13–37, https://doi.org/10.5194/angeo-41-13-2023, 2023.

Kanekal, S. and Miyoshi, Y.: Dynamics of the terrestrial radiation belts: a review of recent results during the VarSITI (Variability of the Sun and Its Terrestrial Impact) era, 2014–2018, Progress in Earth and Planetary Science, 8, 35, https://doi.org/10.1186/s40645-021-00413-y, 2021.

Kelbert, A. and Lucas, G. M.: Modified GIC Estimation Using 3-D Earth Conductivity, Space Weather, 18, e2020SW002 467, https://doi.org/10.1029/2020SW002467, 2020.

Love, J. J. and Chulliat, A.: An International Network of Magnetic Observatories, Eos, Transactions American Geophysical Union, 94, 373–374, https://doi.org/10.1002/2013EO420001, 2013.

Mac Manus, D. H., Rodger, C. J., Dalzell, M., Thomson, A. W. P., Clilverd, M. A., Petersen, T., Wolf, M. M., Thomson, N. R., and Divett, T.: Long-term geomagnetically induced current observations in New Zealand: Earth return corrections and geomagnetic field driver, Space Weather, 15, 1020–1038, https://doi.org/10.1002/2017SW001635, _eprint: https://onlinelibrary.wiley.com/doi/pdf/10.1002/2017SW001635, 2017.

Mac Manus, D. H., Rodger, C. J., Dalzell, M., Renton, A., Richardson, G. S., Petersen, T., and Clilverd, M. A.: Geomagnetically Induced Current Modeling in New Zealand: Extreme Storm Analysis Using Multiple Disturbance Scenarios and Industry Provided Hazard Magnitudes, Space Weather, 20, e2022SW003 320, https://doi.org/10.1029/2022SW003320, 2022.

Madsen, F. D., Beggan, C. D., and Whaler, K. A.: Forecasting changes of the magnetic field in the United Kingdom from L1 Lagrange solar wind measurements, Frontiers in Physics, 10, https://doi.org/10.3389/fphy.2022.1017781, 2022.

Marshall, R. A., Smith, E. A., Francis, M. J., Waters, C. L., and Sciffer, M. D.: A preliminary risk assessment of the Australian region power network to space weather, Space Weather, 9, https://doi.org/10.1029/2011SW000685, 2011.

Matzka, J., Stolle, C., Yamazaki, Y., Bronkalla, O., and Morschhauser, A.: The Geomagnetic Kp Index and Derived Indices of Geomagnetic Activity, Space Weather, 19, e2020SW002 641, https://doi.org/10.1029/2020SW002641, 2021.

Mishra, W. and Teriaca, L.: Propagation of coronal mass ejections from the Sun to the Earth, Journal of Astrophysics and Astronomy, 44, 20, https://doi.org/10.1007/s12036-023-09910-6, 2023.

Oughton, E., Hapgood, M., Richardson, G., Beggan, C., Thomson, A., Gibbs, M., Burnett, C., Gaunt, C., Trichas, M., Dada, R., and Horne, R.: A Risk Assessment Framework for the Socioeconomic Impacts of Electricity Transmission Infrastructure Failure Due to Space Weather: An Application to the United Kingdom, Risk Analysis, 39, https://doi.org/10.1111/risa.13229, 2018.

Pedersen, M. N., Juusola, L., Vanhamäki, H., Aikio, A. T., and Viljanen, A.: Rapid Geomagnetic Variations During High-Speed Stream, Sheath and Magnetic Cloud-Driven Geomagnetic Storms From 1996 to 2023, Journal of Geophysical Research: Space Physics, 129, e2024JA032 656, https://doi.org/10.1029/2024JA032656, 2024.

Pulkkinen, A., Lindahl, S., Viljanen, A., and Pirjola, R.: Geomagnetic storm of 29–31 October 2003: Geomagnetically induced currents and their relation to problems in the Swedish high-voltage power transmission system, Space Weather, 3, https://doi.org/10.1029/2004SW000123, 2005.

Pulkkinen, A., Bernabeu, E., Thomson, A., Viljanen, A., Pirjola, R., Boteler, D., Eichner, J., Cilliers, P. J., Welling, D., Savani, N. P., Weigel, R. S., Love, J. J., Balch, C., Ngwira, C. M., Crowley, G., Schultz, A., Kataoka, R., Anderson, B., Fugate, D., Simpson, J. J., and MacAlester, M.: Geomagnetically induced currents: Science, engineering, and applications readiness, Space Weather, 15, 828–856, https://doi.org/10.1002/2016SW001501, 2017.

Rajput, V. N., Boteler, D. H., Rana, N., Saiyed, M., Anjana, S., and Shah, M.: Insight into impact of geomagnetically induced currents on power systems: Overview, challenges and mitigation, Electric Power Systems Research, 192, 106 927, https://doi.org/10.1016/j.epsr.2020.106927, 2021.

Ramírez-Niño, J., Haro-Hernández, C., Rodriguez-Rodriguez, J. H., and Mijarez, R.: Core saturation effects of geomagnetic induced currents in power transformers, Journal of Applied Research and Technology, 14, 87–92, https://doi.org/https://doi.org/10.1016/j.jart.2016.04.003, 2016.

Rastogi, R. G.: Magnetic storm effects in H and D components of the geomagnetic field at low and middle latitudes, Journal of Atmospheric and Solar-Terrestrial Physics, 67, 665–675, https://doi.org/10.1016/j.jastp.2004.11.002, 2005.

Robertson, R. C.: A Numerical Evaluation of the Limitations of the Thin-Sheet Approximation, IEEE Transactions on Geoscience and Remote Sensing, GE-25, 130–137, https://doi.org/10.1109/TGRS.1987.289812, conference Name: IEEE Transactions on Geoscience and Remote Sensing, 1987.

Smith, A., Forsyth, C., Rae, I. J., Rodger, C., and Freeman, M.: The Impact of Sudden Commencements on Ground Magnetic Field Variability: Immediate and Delayed Consequences, Space Weather, 19, https://doi.org/10.1029/2021SW002764, 2021.

Smith, A. R. A., Pačes, M., and DISC, S.: Python tools for ESA's Swarm mission: VirES for Swarm and surrounding ecosystem, Frontiers in Astronomy and Space Sciences, 9, https://doi.org/10.3389/fspas.2022.1002697, 2022.

Smith, A. R. A., Pačes, M., and Santillan, D.: ESA-VirES/VirES-Python-Client, https://doi.org/10.5281/zenodo.14946149, 2025.

Thompson, R.: Geomagnetic field: Westward drift, in: Geophysics, pp. 507–511, Springer US, Boston, MA, ISBN 978-0-387-30752-7, https://doi.org/10.1007/0-387-30752-4_63, 1990.

Thomson, A. W. P., Dawson, E. B., and Reay, S. J.: Quantifying extreme behavior in geomagnetic activity, Space Weather, 9, https://doi.org/10.1029/2011SW000696, 2011.

Usoskin, I. G. and Kovaltsov, G. A.: Occurrence of extreme solar particle events: assessment from historical proxy data, The Astrophysical Journal, 757, 92, https://doi.org/10.1088/0004-637X/757/1/92, 2012.

Viljanen, A.: Relation of geomagnetically induced currents and local geomagnetic variations, IEEE Transactions on Power Delivery, 13, 1285–1290, https://doi.org/10.1109/61.714497, conference Name: IEEE Transactions on Power Delivery, 1998.

Viljanen, A., Nevanlinna, H., Pajunpää, K., and Pulkkinen, A.: Time derivative of the horizontal geomagnetic field as an activity indicator, Annales Geophysicae, 19, 1107–1118, https://doi.org/10.5194/angeo-19-1107-2001, 2001.

Zhang, H. X., Lu, J. Y., and Wang, M.: Energy transfer across magnetopause under dawn–dusk IMFs, Scientific Reports, 13, 7409, https://doi.org/10.1038/s41598-023-34082-2, 2023.